PERGAMON

Vision Research 39 (1999) 3386–3398

Vision Research

www.elsevier.com/locate/visres

Use of an early nonlinearity to measure optical and receptor resolution in the human infant

T. Rowan Candy [a,b,*], Martin S. Banks [a]

[a] *School of Optometry, University of California at Berkeley, Berkeley, CA, USA*
[b] *The Smith-Kettlewell Eye Research Institute, 2318 Fillmore Street, San Francisco, CA 94115, USA*

Received 23 July 1998; received in revised form 5 January 1999

Abstract

We measured the resolution of the optics and receptoral processes in human infants. To do so, we recorded visual-evoked potentials (VEPs) to sampled sinewave gratings, stimuli that generate highly visible distortion products at a nonlinearity early in the retina. We varied the spatial frequency content of the stimulus to determine the frequencies that can be transmitted through the optics and receptors and thereby generate distortion products. Data were collected from adults and 2- to 7-month-old infants. The results indicated that the resolution of the infants' optical/receptoral processes was within a factor of two of adults' even at the earliest ages tested. These first stages of processing, therefore, do not explain infants' poor performance in many visual tasks, or restrict the types of visual stimuli affecting more central mechanisms that undergo experience-dependent development.

Keywords: Human infant; Visual acuity; Optics; Photoreceptors; Nonlinear distortion

1. Introduction

Recent models of human visual development have examined the extent to which infants' low visual acuity and spatial contrast sensitivity can be understood from information losses among the optics and photoreceptors (Brown, Dobson & Maier, 1987; Banks & Bennett, 1988; Wilson, 1988, 1993; Banks & Crowell, 1993; Brown, 1993; Candy, Banks, Hendrickson & Crowell, 1993). Such analyses are important for two reasons. First, the optical and receptor stage is common to all aspects of vision, so an understanding of how optics and receptors constrain the transmission of visual inputs to more central circuits could help us understand infants' visual performance in a wide range of tasks (Banks & Bennett, 1988). Second, the postnatal development of central neural circuits is dependent upon the information transmitted to them (Lam & Shatz, 1991), so an understanding of the information available at the receptor outputs may help us better understand the role of visual experience in guiding development.

These modeling studies used the spatial contrast sensitivity function (CSF) as the primary performance index. Most concluded that optical and photoreceptor immaturities in the neonate impose significant limitations on contrast sensitivity, but that they alone are insufficient to explain the low contrast sensitivity of the visual system as a whole (Banks & Bennett, 1988; Banks & Crowell, 1993; Brown, 1993; but see Wilson, 1988). However, these models made some unverified assumptions because some properties of the optics and photoreceptors in the neonate are unknown. For this reason, the aim of the current study was to measure the spatial resolution of the optics and receptors of human infants.

As noted by MacLeod and colleagues (MacLeod, Williams & Makous, 1992; Chen, Makous & Williams, 1993; MacLeod & He, 1993), the visual system can be modeled as a series of filters: a linear spatiotemporal filter, followed by a nonlinearity, and then by a second spatiotemporal filter. MacLeod and colleagues used distortion products created by the nonlinearity to measure the spatial properties of the first and second linear filters in human adults. They showed that the nonlinearity lies early in the retina, probably at the photore-

* Corresponding author. Fax: +1-415-3458455.
E-mail address: rowan@skivs.ski.org (T.R. Candy)

0042-6989/99/$ - see front matter
PII: S0042-6989(99)00035-8

ceptor outputs. We used distortion products created by this early nonlinearity to measure the spatial resolution of the first linear filter in human infants.

To study the properties of the first and second linear filters, MacLeod and colleagues bypassed the eye's optics using laser interferometery. Thus, their measurements reflect the spatial filtering properties of the neural parts of the first filter alone. For the adult fovea, they reported a spatial integration diameter at the input to the nonlinear site of ~ 15 arcsec (MacLeod et al., 1992; Chen et al., 1993; MacLeod & He, 1993); Because this resolution is slightly smaller than the inner segment diameter of a single foveal cone (Curcio, 1987), they concluded that signals from individual cones are preserved at the input to the nonlinearity.

In the current study, stimuli were presented using conventional optics. Thus, our results reflect the contributions of filtering due to the optics and all neural elements prior to the nonlinearity.

1.1. The stimulus

We used a stimulus developed by Burr, Ross and Morrone (1985). This sampled grating stimulus is a low spatial-frequency sinewave multiplied by a sampling function. Its one-dimensional luminance profile is shown in Fig. 1; it is described by the following equation:

$$l(x, y) = \frac{L_p}{w}[1 + m \cos 2\pi f_0 y] \cdot \left[\mathrm{comb}\left(\frac{y}{S}\right) * \mathrm{rect}\left(\frac{y}{w}\right) \right]$$

where $\cdot$ and * represent multiplication and convolution respectively, y is vertical position, L_p is mean luminance, f_0 is the sinewave's spatial frequency, m is the sinewave's Michelson contrast, w is sample width, and S is centre-to-centre spacing of the samples. Examples of the sampled grating stimulus are shown in Fig. 2.

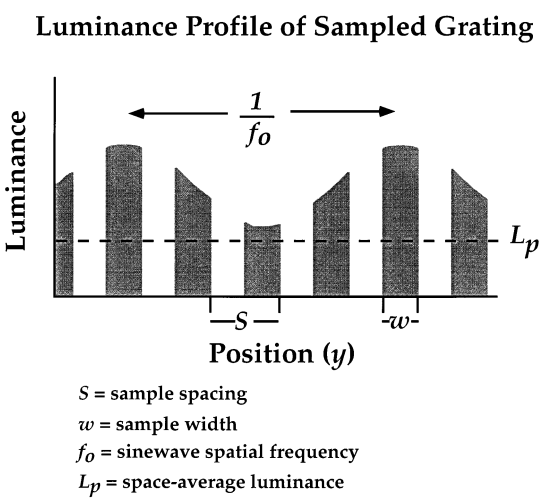

Fig. 1. Luminance profile of sampled sinewave grating. Luminance is plotted as a function of vertical position. Displayed parameters are: vertical stimulus position (y), space-average luminance (L_p), sample width (w), sinewave spatial frequency (f_0), and sample spacing (S).

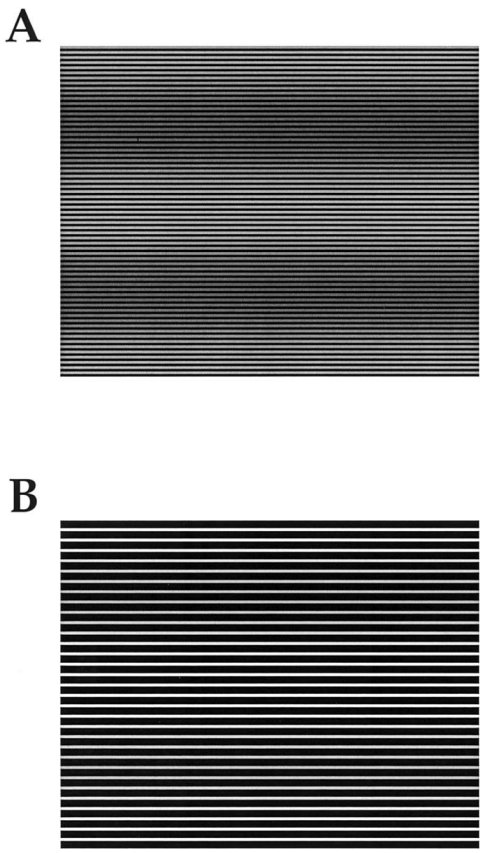

Fig. 2. Examples of sampled gratings. The spatial frequency of the sinewave is two cycles per panel in both A and B; the amplitudes are the same. In A, the sample spacing is twice the sample width and in B, it is four times the sample width. While you inspect the two panels, increase and decrease the viewing distance. Notice that the visibility of the sinewave in the upper panel is always equal to or greater than the visibility of the sinewave in the lower panel. See text for explanation. This reproduction is not entirely accurate as it is subject to nonlinearities in the printing process.

We measured detection thresholds for the sinewave as a function of sample spacing; sample width and mean luminance were constant. The relationship between the samples and the sinewave was constrained in the following ways: The samples were aligned with peaks and troughs of the sinewave modulation, more than two samples were present for each sinewave period, and the number of samples per period was a power of two. Luminance profiles of some of the stimuli are shown in Fig. 3. Panels A–C depict an unsampled sinewave, a sinewave with narrow sample spacing, and one with wide sample spacing, respectively. As sample spacing was increased, sample luminance was increased in order to maintain constant space-average luminance.

1.2. The theoretical approach

As mentioned earlier, we made use of a static nonlinearity early in the retina to isolate the resolution of the first linear filter (presumably, the optics and receptors). We represent the visual system as a series of filters: an initial linear filter, a nonlinearity, and a subsequent linear filter (Burton, 1973; MacLeod et al., 1992), A linear filter's output contains only spatial frequencies that are in the input, but a nonlinearity creates additional spatial frequency components—distortion products—including the sums and differences of the input components (Burton, 1973). The creation of such distortion products is the key to our approach. To explain this, we first describe the sampled grating stimulus in the Fourier domain.

Fig. 4 depicts a linear filter and the amplitude spectra for the sampled gratings shown in Fig. 3. The amplitude spectrum is determined from the Fourier transform of the stimulus:

$$L(f) = L_p \sum_{n=-\infty}^{\infty} \delta\left(f - \frac{n}{S}\right)\mathrm{sinc}(wf) + L_p m\left[\frac{1}{2|f_0|}\delta\delta\left(\frac{f}{f_0}\right) \times {}^{*}\left[\sum_{n=-\infty}^{\infty} \delta\left(f - \frac{n}{S}\right)\mathrm{sinc}(wf)\right]\right]$$

where f is spatial frequency, $\mathrm{sinc}(wf)$ is $\sin \pi wf / \pi wf$ and $\delta\delta$ is the Fourier transform of the cosine function.

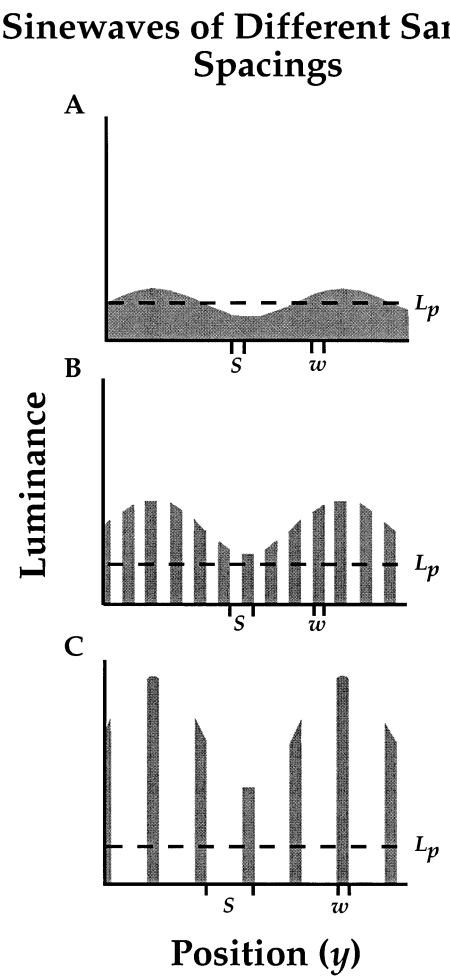

Fig. 3. Luminance profiles of sampled sinewave gratings at different sample spacings. S, w, and L_p defined in Fig. 1 and text. Sinewave amplitude, sample width and average luminance are the same in each panel. (A) Conventional sinewave grating; sample spacing equals sample width. (B) Sample spacing is twice sample width. (C) Sample spacing is four times sample width.

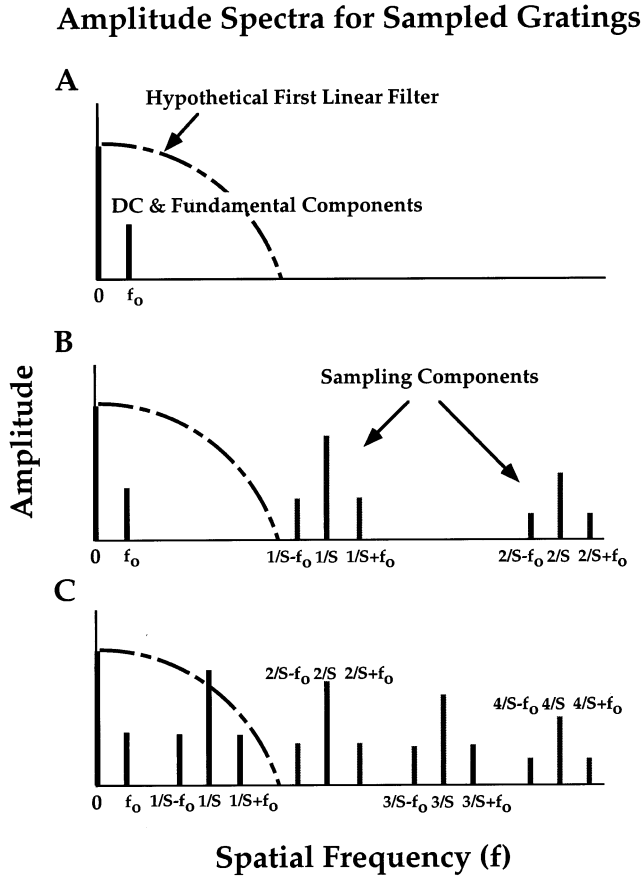

Fig. 4. The first linear filter and amplitude spectra of sampled sinewave gratings. Amplitudes of Fourier components are plotted as a function of spatial frequency. Each panel displays the amplitude spectra for a different sample spacing; the three stimuli are the ones in Fig. 3. The transfer function of the hypothetical first linear filter is also shown in each panel. (A) Conventional sinewave grating; sample spacing equals sample width and so the spectrum consists only of a DC component and the Fourier fundament at f_0. (B) Sample spacing is twice the sample width. The spectrum contains the DC component and Fourier fundamental as before, but it now also contains triplets of sampling components centered at $1/S$, $2/S$, and so forth. The spatial frequencies of the sampling components are all higher than the passband of the linear filter, so they do not penetrate this processing stage. (C) Sample spacing is four times sample width. The spectrum again contains the DC and fundamental, and triplets of sampling components centered at $1/S$, $2/S$, etc. The spatial frequencies of the first triplet are now low enough to penetrate the linear filter, so they are passed to the nonlinearity.

The amplitude spectrum for a conventional sinewave (Fig. 4A) consists of a DC component and a component at the sinewave spatial frequency, f_0; the latter is the fundamental frequency. Sampling the sinewave in the fashion shown in Figs. 1–3 yields additional components at multiples of the sampling frequency (n/S), and sidebands at $((n/S)-f_0)$ and $((n/S)+f_0)$. We will refer to these additional components as the sampling components. The entire spectrum has also been multiplied by a sinc(wf) function which is determined by the sample width.

Now consider the spectrum as it is passed by the linear filter. If the sampling component frequencies are higher than the passband of the filter (i.e. the sampling is spaced too finely), they will not reach the nonlinearity. Consequently, from the standpoint of subsequent processing stages, the input is identical to that of a conventional unsampled sinewave. This situation is depicted in Fig. 4B (the sampling components do not penetrate the linear filter).

As the frequencies of the sampling components are reduced (by increasing the sample spacing), they eventually pass through the first filter and reach the nonlinearity (Fig. 4C). A nonlinearity creates distortion products at the sums and differences of the input frequency components (Chen et al., 1993). The difference between the sampling components and their sidebands, $n/S-(n/S\pm f_0)$, is always the spatial frequency of the fundamental, f_0. As a consequence, when the sampling components pass through the first filter, the nonlinearity produces distortion products at frequency f_0. Depending on the phases of these components, they will add to, or subtract from, the amplitude of f_0.

According to the theoretical approach presented here, when one measures the detectability of f_0, the threshold should be constant across a range of narrow sample spacings because with narrow spacing the sampling components cannot penetrate the first linear filter; they, therefore, cannot affect the detectability of f_0. As the sample spacing is increased, the spatial frequencies of the sampling components are reduced until they penetrate the linear filter. They reach the nonlinearity and, if the sampling components have sufficient amplitude, they create distortion products at f_0 that can now affect detectability. Detection threshold will rise or fall depending on the form of the nonlinearity. It will rise if the nonlinearity is compressive, because the phase of the distortion products is 180° relative to f_0 (Green, 1976). It will fall if the nonlinearity is expansive. The threshold data do not depend on the spatiotemporal properties of the post-nonlinearity filter(s) because that part of the visual system is always presented the same stimulus f_0.

1.3. The results of Burr, Ross and Morrone (1985)

Burr et al. (1985) used the sampled sinewave stimulus to examine local gain control in the human visual system. For their purposes, they analysed their results in terms of samples per sinewave cycle, rather than sample spacing per se. Nonetheless, the consequences of nonlinear distortion should be apparent in their data. To examine this possibility, we replotted their data as a function of sample spacing; Fig. 5 shows their data plotted with each point expressed relative to the unsampled contrast threshold at that spatial frequency. Threshold is constant across a range of narrow sample spacings, and then rises monotonically for spacings greater than 1–2 minarc. Notice that the form of the threshold functions is essentially the same for all sinewave spatial frequencies. We will refer to the sample spacing at which threshold begins to rise as the *critical sample spacing*. According to the theoretical approach outlined above, the threshold elevation occurs when the spatial frequencies of the sampling components are low enough to penetrate the first linear filter. Distortion products are then created at the nonlinearity and threshold rises, because some of those products reduce the effective amplitude of the fundamental of the sinewave.

There are other possible interpretations for these data. Perhaps the threshold elevation is due to conventional spatial-frequency masking (e.g. Stromeyer & Julesz, 1972). However, if this were so, critical sample spacing should vary with the sinewave frequency and it does not. For this reason, conventional spatial-frequency masking cannot explain the data.

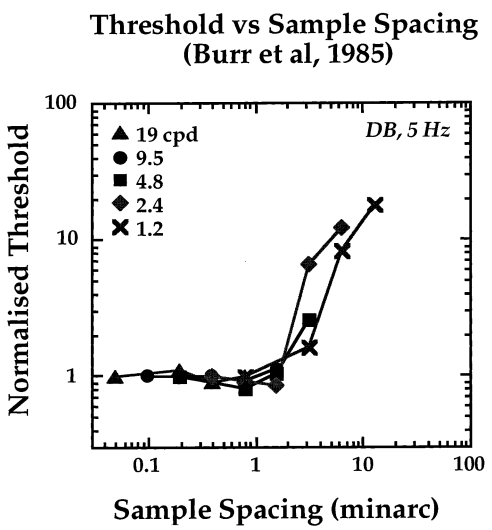

Fig. 5. Data from Burr et al. (1985). Normalised thresholds are plotted as a function of sample spacing. Different symbols represent thresholds obtained at different sinewave frequencies. The threshold data have been normalised by dividing each threshold value by the contrast threshold for a conventional sinewave grating of the same spatial frequency ($S=w$).

What visual processes cause threshold to rise at 1–2 minarc in the Burr et al. data? If we assume that the critical sample spacing is a measure of the summation width of the first linear filter, then the estimated width is considerably larger in the data of Burr et al. (1985) than in those of MacLeod et al. (1992) who reported an integration diameter of $\sim$15 arcsec in the fovea. Recall, however, that MacLeod and colleagues used interferometry to bypass the optics, so they measured the first filter uncontaminated by optical degradation. In contrast, the measurements of Burr et al. include optical filtering, so their measurements reflect the contributions of optics and neural filtering together; indeed, their results are consistent with Campbell and Gubisch's (1966) estimate of the optical point spread function for a 2-mm pupil.

We first sought to confirm that the threshold elevation observed in the Burr et al. data manifests the spatial resolution of the first filter. We did this by conducting a series of experiments in adults. We then used the approach to examine 2- to 7-month-old infants.

2. General methods

2.1. Apparatus and procedure

The stimuli were generated using a Nuvista[1] graphics board in an Apple Power Macintosh 7100/80AV. They were presented on a Dotronix monochrome monitor. The monitor was calibrated regularly to compensate for screen nonlinearities. The sinewave grating and samples were oriented horizontally in order to avoid the adjacent pixel nonlinearity (Klein, Hu & Carney, 1996). Space-average luminance was 12 cd/m^2 in all experiments. This low value was chosen so that we could render the bright samples needed at wide sample spacings. An ISR[2] video attenuator was also used so we could present the low contrasts required for adult psychophysics (Pelli & Zhang, 1991). The stimulus patch was defined by a circular aperture 4° in diameter. Sample widths (w) were always one pixel, which corresponded to 0.5–1.6 minarc at the viewing distances used.

3. Adult foveal experiment

The aim of the first experiment was to replicate the results of Burr et al. (1985). Foveal thresholds were measured for sinewave frequencies from 0.45–7.5 c/deg.

3.1. Methods

The adult observers were two emmetropes, 20 and 27 years old; one of the authors and a naive observer. They were cyclopleged (two drops of 0.5% Cyclogyl administered 5 min apart), and tested monocularly with a 2-mm artificial pupil and best optical correction for the stimulus. Cycloplegia was used to assure accurate accommodation and maximum resolution of the first linear filter. The observers' heads were stabilised with a bite bar. Viewing distance was 325 cm (where one pixel subtended 0.5 minarc).

The observers viewed a small fixation point in the center of the display. Thresholds were estimated using a two interval, forced-choice procedure. The two intervals consisted of 240-ms presentations of a sampled sinewave grating and a sampled uniform field of the same space-average luminance and sample spacing. The observers' task was to identify the interval containing the sinewave. The amplitude of the sinewave was varied according to the method of constant stimuli. At least 200 trials were presented for each threshold estimate. The 75% correct point was estimated by fitting a Weibull function to the psychometric data. This point served as the threshold estimate.

3.2. Results

The left panels in Fig. 6 plot foveal thresholds as a function of sample spacing for the two adult observers. The thresholds have been normalised by dividing each threshold estimate by the average threshold for the two narrowest sample spacings at the same spatial frequency. Thresholds for the unsampled sinewaves varied with sinewave spatial frequency in the fashion expected from the conventional CSF. The normalised data form very similar curves at the various sinewave frequencies; in each case, the critical sample spacing is $\sim$2 minarc. These data are quite consistent with the results of Burr and colleagues and indicate a linear filter resolution of $\sim$2 minarc.

Again the similarity of the threshold functions and critical sample spacings in Figs. 5 and 6 strongly suggests that the threshold elevation is not caused by conventional spatial frequency masking. These data are, therefore, consistent with the theoretical approach outlined earlier.

4. Adult peripheral experiment

The foveal results described above do not allow us to pinpoint the anatomical location of the nonlinearity because there is little if any pooling of foveal cones onto higher-order retinal neurons (Wässle, Grünert, Röhrenbeck & Boycott, 1990). However, in the

[1] Truevision, 7340 Shadeland Station, Indianapolis, IN 46256.

[2] Video Attenuator from the Institute for Sensory Research, Syracuse University, Syracuse, NY 13244.

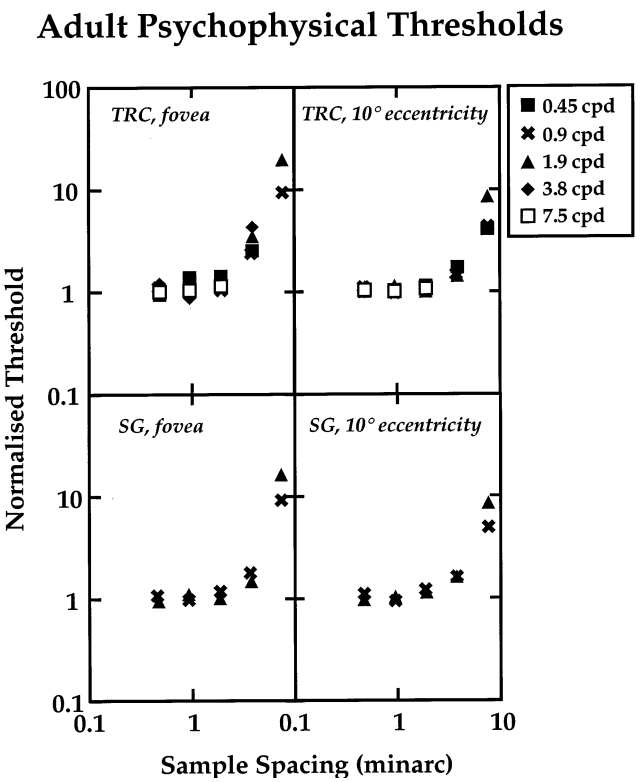

Fig. 6. Adult psychophysical thresholds. Normalised threshold is plotted as a function of sample spacing. Different symbols represent thresholds at different sinewave frequencies. Data from observers TRC and SG are displayed in the upper and lower panels, respectively. Data from the fovea and from a retinal eccentricity of 10° are plotted in the left and right panels, respectively. Data were normalised by dividing threshold estimates by the average threshold for the two narrowest sample spacings.

parafovea and periphery, there are more cones than bipolar and retinal ganglion cells; cones are pooled to form larger receptive fields among these cell types (Wässle et al., 1990). Chen et al. (1993) repeated their experiment at retinal eccentricities of 3.8 and 30°. They found that the diameter of the spatial integration area was approximately 40 arcsec at 3.8° and 50 arcsec at 30°. These values are similar to, or even smaller than, the aperture of individual cones at those retinal eccentricities. Thus, Chen et al. concluded that there was no evidence for summation of signals prior to the nonlinear process and, therefore, that the linear filter assessed by their technique is the photoreceptor itself and that the nonlinearity is at the receptor output or the input to the bipolars.

We collected data at a retinal eccentricity of 10° to determine whether the nonlinearity driven by our sampled-grating technique also lies at the receptor outputs or nearby. As stated, we did not bypass the optics of the eye, but the optical point spread function does not differ significantly between the fovea and 10° (Navarro, Artal & Williams, 1993), so the image quality at the eccentric point should be quite similar to the quality at the fovea. Thus, if the nonlinearity lies before the convergence of cones onto higher-order retinal neurons, the critical sample spacing should be similar in the fovea and at 10°. If, however, the nonlinearity lies after neural convergence, critical sample spacing should be much finer in the fovea than at 10°.

Except for the change in retinal eccentricity, the stimuli and procedure were the same as before.

4.1. Results

The grating acuities of observer TRC were 43 c/deg in the fovea and 14 c/deg at 10°. Thus, the resolution of the visual system as a whole was much lower at the eccentric retinal locus. Given the similarity of the optical point spread function at the two retinal loci, the non-foveal acuity loss is presumably a manifestation of receptor pooling onto higher-order neurons (Banks, Sekuler & Anderson, 1991).

The right panels in Fig. 6 show the normalised thresholds at 10° retinal eccentricity for the two adult observers. Notice that the critical sample spacing increased only slightly from the foveal to the peripheral measurements. This finding, compared with the large change in grating acuity suggests strongly that the critical sample spacing is a measure of the resolution of the combined optics and photoreceptors and not that of higher-order retinal neurons or more central visual circuits. The result is, therefore, consistent with the theory presented above.

5. Adult optical defocus experiment

We conducted one further validation experiment by measuring the effects of artificially reducing the resolution of the linear filter. When the resolution of the filter is reduced, our theoretical approach predicts that the critical sample spacing should increase. To test this prediction, foveal data were collected from one observer with two levels of optical defocus: +2 and +3 dioptres. Thresholds were measured using the same stimuli and procedure as before.

5.1. Results

The results are shown in Fig. 7. The squares, crosses, and triangles represent thresholds obtained with the three levels of optical defocus: 0, +2, and +3D, respectively. According to the theory presented above, critical sample spacing should increase with increasing defocus. This effect is evident in the data: The critical sample spacing is clearly greater with +2 and +3D of defocus than at 0D. The fact that critical sample spacing increases with increasing optical defocus supports our argument that the critical spacing value is a mea-

sure of the resolution of the processes before the first nonlinearity.

It is interesting to note that defocus actually improves performance in this task. Note, for example, the thresholds at a sample spacing of 8 minarc. With 0D defocus, threshold was nearly a log unit higher than with +3D defocus.

It would be convenient to be able to represent critical sample spacing in terms of equivalent blur (Levi & Klein, 1990). Unfortunately, critical sample spacing measured with our technique is affected by both the bandwidth of the first linear filter and the shape of the nonlinear transducer function. A severely compressive nonlinearity produces distortion products when sampling frequencies are barely passed by the linear filter. With a less compressive nonlinearity, the sampling frequency components must be higher in amplitude in order to create significant distortion products. Thus, we cannot represent critical sample spacing by an equivalent blur.

6. Infant experiment

The human infant experiment was conducted by recording the visual-evoked potential (VEP). We chose this technique because it seemed unlikely that the forced-choice preferential looking paradigm (Teller, 1979) could be adapted for the measurements required here. (It is unlikely that infants would preferentially fixate the low-contrast grating when the high-contrast sampling function is present in both stimuli.)

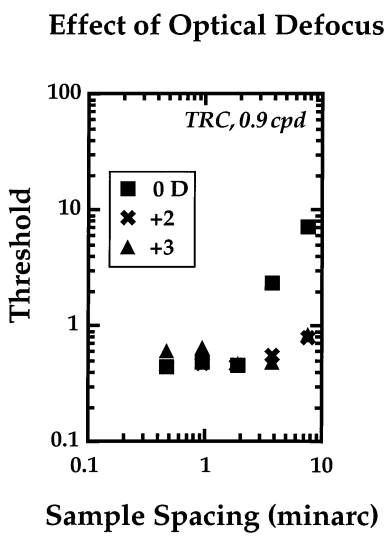

Fig. 7. Effect of optical defocus on detection of sampled sinewaves. Normalised threshold is plotted as a function of sample spacing and amount of optical defocus. The spatial frequency of the sinewave was 0.9 c/deg. Squares, crosses, and triangles represent the data with 0, +2, and +3D of defocus, respectively.

6.1. Methods

The stimuli were the same as those in the adult experiments and were generated with the same equipment. We used the sweep VEP technique (Norcia, Clarke & Tyler, 1985; Norcia & Tyler, 1985; Norcia, Tyler, Hamer & Wesemann, 1989). Thresholds were measured for a variety of sample spacings and sinewave frequencies. The sinewave was pattern-reversed, but the sample positions did not alternate, so any evoked response must reflect response to the sinewave rather than to the samples.

The EEG was recorded using Grass gold-cup electrodes and Grass Model P511K amplifiers with gains of 50 000 in adults and 10 000 or 20 000 in infants (depending on their level of muscle activity). Responses were recorded from two bipolar channels over the visual cortex; O1 and O2, both referred to OZ, with a ground electrode placed at CZ (following the ten-twenty electrode system; Jasper, 1958). The skin was initially prepared by rubbing each electrode position with Omniprep skin preparation cream, and the electrodes were secured in place with Grass EC2 electrode cream, gauze, and a headband. The data were analysed using a MacDSP[3] board synchronised with the stimulus generation board.

Comparison VEP data were collected from adults before testing infants. The adults were three naive observers aged 20–35 years. The infants were recruited through city birth records. All infants were born within 2 weeks of their due date with no abnormalities or complications noted at birth. Also, no significant ocular abnormalities were detected at data collection.

Data were collected from infants in one-hour sessions with the informed consent of their parents. A small number of infants returned for additional visits to provide reliability data, but most participated in only one session. Including pilot testing, 61 infants were tested; data from 27 of them were included in the final analysis. Any infant who did not provide thresholds for at least three of the five sample spacings at one sinewave frequency, in a single session, was excluded from this final analysis. These infants were fussy, had poor VEP responses, or fell asleep.

Infants were tested at 1 m (where one pixel subtended 1.6 minarc), and adults were tested at 1.5 m (where one pixel subtended 1.1 minarc). The stimulus was not masked by the circular aperture in this main experiment; it subtended $17 \times 13°$ for infants and $12 \times 8°$ for adults.

All subjects viewed the stimulus binocularly. Adults wore their best optical correction for the viewing distance and were encouraged to focus on a small central

[3] Spectral Innovations Inc., 4633 Old Ironsides Drive Ste. 401, Santa Clara, CA 94054.

fixation target. Infants were not optically corrected and were merely encouraged to fixate the screen center where a small toy was placed to attract their attention. The experimenter moved the toy to encourage fixation and would pause data collection whenever the infant was not fixating accurately. Because we had no means to assure accurate accommodation in the infants, they may have experienced artifactual optical defocus; this point will be discussed in greater detail later.

Five trials were conducted at each sample spacing. During a trial, the sinewave's amplitude was increased logarithmically over 10.6 s; the amplitude was incremented every 1.06 s, so it took on ten values during a trial. The sinewave amplitude range for each trial was chosen such that the threshold value was presented approximately 3–4 s after the start of the trial. The raw responses were analysed using the discrete Fourier transform. With pattern reversal, the largest response occurs at the second harmonic, so response at that harmonic was plotted as a function of the logarithm of stimulus amplitude. Thresholds were then estimated by linear extrapolation of the response versus log amplitude plots. The threshold was the point at which the best-fitting line reached zero voltage. The average voltage response from the five trials was also calculated by coherently averaging sine and cosine response components at each stimulus amplitude. An average threshold for each sample spacing was then obtained from these averaged data by linear extrapolation as described above.

The younger infants (8–14 weeks) were tested with a pattern-reversal rate of 3.3 Hz and the older infants (14–28 weeks) were tested with a rate of 6.6 Hz[4]. We used different rates because the reversal rate at which the lowest thresholds are obtained increases with age (Sokol, Moskowitz, McCormack & Augliere, 1988).

In a control experiment, we presented several trials to adults while holding stimulus amplitude constant for the entire 11-s trial. The aim was to determine if adaptation occurred during the course of a trial. If adaptation occurred, threshold estimates obtained by our extrapolation procedure would be affected by the range of amplitudes presented during a sweep and the rate at which amplitude is varied during a trial. Fortunately, we found that no discernible adaptation occurred.

6.2. Results

Foveal VEP data from adult observers are shown in Fig. 8. Data from the three observers are presented in rows, and data from two sinewave spatial frequencies—0.85 and 1.7 c/deg—are presented in columns. The pattern-alternation rate was 6.6 Hz. The open squares represent thresholds from individual trials and the solid squares thresholds from averaged responses. These data exhibit threshold elevations at sample spacings of ~2 minarc and larger; this is comparable to the foveal psychophysical data.

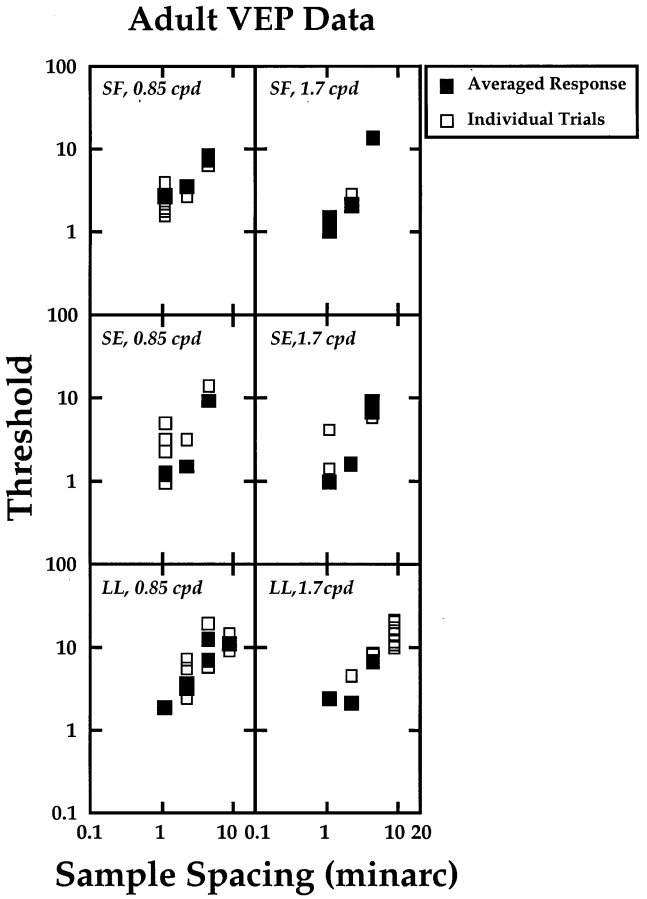

Fig. 8. Adult VEP thresholds. Normalised threshold is plotted as a function of sample spacing. Data from observers SF, SE, and LL are displayed in the upper, middle, and lower panels, respectively. Data with the sinewave frequency set to 0.85 and 1.7 c/deg are plotted in the left and right panels, respectively. Unfilled symbols represent thresholds calculated from individual VEP trials and filled symbols thresholds calculated from the averaged response at each sample spacing.

The infant data, grouped by age, are shown in Fig. 9. The individual data[5] (unfilled symbols) are quite variable, so we also show the group-average data (filled symbols) for each age group.

Fig. 9 reveals that the effect of sample spacing on threshold is nearly adult-like at even the earliest age

[4] MacLeod and He (1993) reported that the distortion products created by the nonlinearity can be created at temporal frequencies as high as 30 Hz.

[5] If an individual infant provided good signals on both channels, the thresholds calculated from the two channels were averaged. If an individual infant provided good signals on one channel only, the threshold from this channel was plotted. Thus, each unfilled square represents the threshold estimate from one infant.

tested (8–10 weeks). Thresholds are relatively constant at small sample spacings and increase monotonically beyond a certain value.

One can estimate the critical sample spacing by fitting the data with two lines, one constrained to have a slope of zero (to fit the data at small sample spacings) and one constrained to have a positive slope (to fit the data at large spacings). We used a nonlinear regression technique to fit the data with the equations:

$$y = a \quad \text{for } x \le c$$
$$y = a + b \times (x - c) \quad \text{for } x > c$$

where x and y are the sample spacing and threshold values, respectively, and constants a, b, and c are free parameters. The constant a is the threshold at narrow sample spacings. The constant b was constrained to be positive and is the slope of the threshold elevation. The best-fitting lines intersect at $x = c$, so c served as the estimate of the critical sample spacing. The critical sample spacing values obtained by this method were 4.75 minarc (S.E. 4.59–4.91), for the data at 8–10 weeks, 1.98 minarc (1.15–3.41) at 10–14 weeks, 4.32 minarc (3.69–5.06) at 14–18 weeks, and 3.2 minarc (2.72–3.77) at 19–28 weeks. Thus, there was no systematic change in the critical sample spacing across the four infant age groups. These values are conservative estimates of the critical sample spacing because the intersection of the two lines typically occurs at a wider spacing than the first threshold elevation.

We collected data from two infants—HB and ZH—at both 3.3 and 6.6 Hz to determine if the choice of temporal frequency affected the estimates of critical sample spacing. These data, shown in Fig. 10, do not exhibit a consistent effect of temporal frequency.

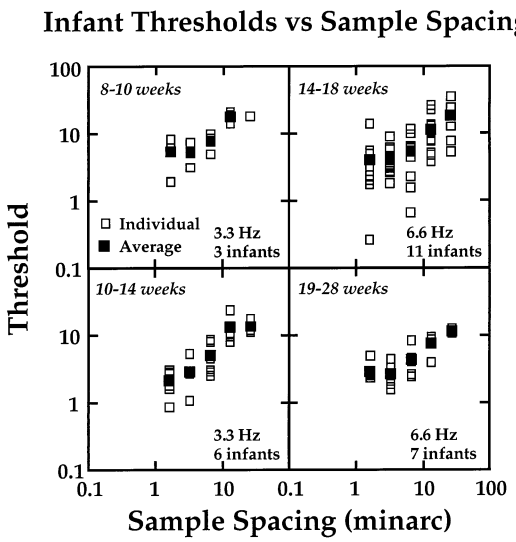

Fig. 9. Infant VEP thresholds. Thresholds are plotted as a function of sample spacing. The four panels show the individual and group-average data from each of four age groups: 8–10 weeks, 10–14 weeks, 14–18 weeks, and 19–28 weeks. The individual data are represented by the unfilled symbols and the group-average data by the filled symbols. The spatial frequency of the sinewave target was 0.3 c/deg and the temporal frequency was the value indicated in each panel.

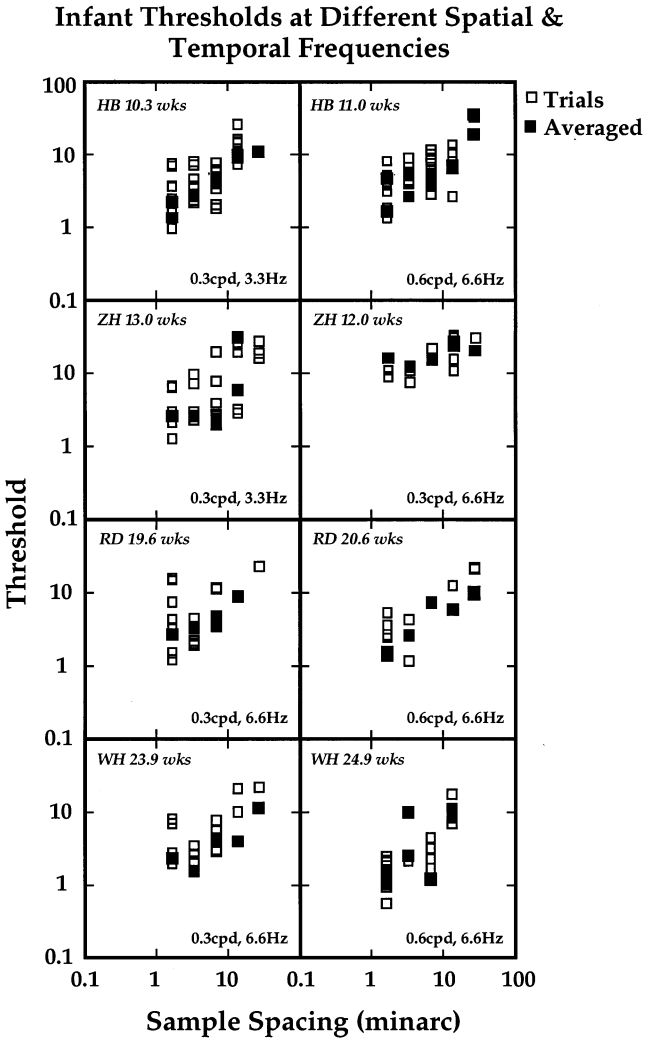

Fig. 10. Individual infant thresholds. Thresholds are plotted as a function of sample spacing for four infants. Each row of panels shows data from a different infant. Unfilled symbols represent threshold estimates obtained on single trials and filled symbols thresholds obtained by averaging trials. The spatial frequency and temporal frequency used to obtain the data are stated in each panel.

The sinewave spatial frequency was 0.3 c/deg for the measurements displayed in Fig. 9. To see if there is any effect of sinewave frequency on the critical sample spacing, we tested three infants at 0.3 and 0.6 c/deg. The data, which are also shown in Fig. 10, exhibit no systematic change in critical sample spacing. This suggests that the threshold elevations we observed are not caused by conventional spatial-frequency masking.

In order to compare the estimated resolution of the first filter to that of the whole visual system, we measured conventional grating acuity from several infants who were still cooperative at the end of the session. We used the standard sweep VEP technique for assessing

grating acuity (Norcia & Tyler, 1985). The stimuli were spatial sinewave gratings of 80% contrast. The estimated acuities are shown as a function of age in Fig. 11. Each point represents the estimated acuity from an individual infant; squares represent acuities when the pattern-alternation rate was 3.3 Hz and crosses represent acuities when it was 6.6 Hz. These data agree well with those of Norcia and Tyler (1985).

Fig. 12 displays critical sample spacing and grating acuity as a function of age. The units on the ordinates are minutes of arc in both cases. The critical sample spacing estimates were obtained using the nonlinear regression analysis described above.

Although acuity and critical sample spacing are plotted with the same units, there is no reason to believe that they will have the same values. For example, the adult foveal values are dissimilar: Critical sample spacing is ~ 3 minarc, but grating acuity is ~ 2 minarc[6]. Of most interest is how the two measures change as a function of age. Although the critical sample spacing estimates are variable, they do not decrease significantly with age. Thus, the resolution of the linear filter does not seem to change dramatically from 2 months of age to adulthood. This finding is noteworthy because many potential artifacts, such as poor accommodation or variable fixation, would probably cause an increase rather than decrease in the estimated critical sample spacing. Furthermore, the lack of a clear developmental change in critical sample spacing is not due to an inadequate range of ages tested or imprecision in our measurements because VEP grating acuity changes quite significantly, perhaps five-fold, over the same age range. We conclude that the resolution of the first linear filter is relatively adult-like at the earliest age tested, and that the primary cause of the development in the acuity of the visual system as a whole is improved resolution among circuits at or higher than the nonlinearity.

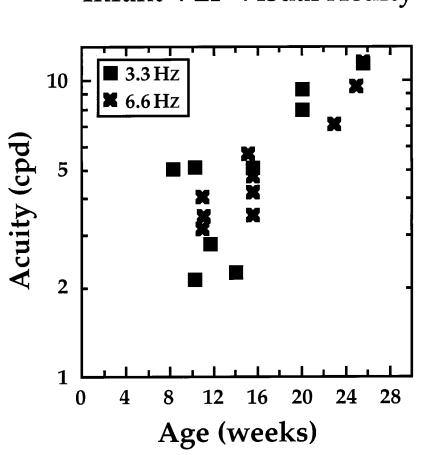

Fig. 11. Infant VEP acuity as a function of age. The spatial frequency of the acuity estimate is plotted as a function of age in weeks. The squares and crosses represent acuities obtained with alternation rates of 3.3 and 6.6 Hz, respectively.

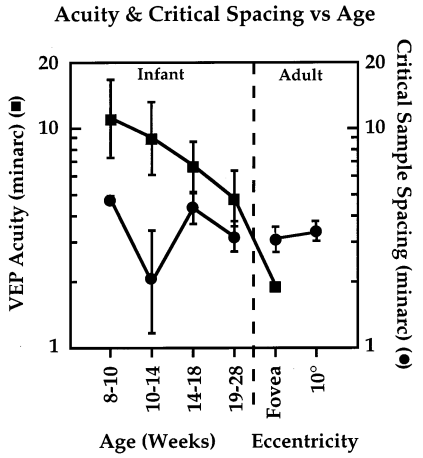

Fig. 12. Grating acuity and critical sample spacing as a function of age. The left panel shows infant data and the right shows adult data. The abscissa on the left represents age in weeks and the one on the right indicates the retinal eccentricity of the adult data. The left ordinate represents grating acuity in minarc. The acuities (minarc per cycle of the grating) are represented by the squares; the infant acuities are derived from Norcia and Tyler (1985), Table 2, but have been averaged into the four age groups on the abscissa. The adult acuity value is from Norcia, Tyler and Hamer (1990). We used Norcia and colleagues' data rather than our own measurements because they tested many more subjects using the same technique. The right ordinate represents critical sample spacing in minarc; the estimates were obtained in the fashion described in the text. We were not able to fit the model to the adult VEP data because of technical limitations on the number of sample spacings we could present. Hence, the adult critical sample spacings are averages of the two observers' psychophysical estimates. The estimated critical sample spacings are represented by the circles. Error bars represent the standard error of the estimate.

7. Discussion

7.1. The critical loss(es) in infant vision

A key issue in the study of visual development is to pinpoint the sites in the visual pathway that are responsible for the low acuity and sensitivity of the human neonate. Our observations are directly relevant to this endeavor.

We observed visual effects—threshold elevations—at sample spacings of 2–5 minarc in 2- to 7-month-old infants. Expressed in the Fourier domain, spacings of 2

[6] There are three reasons that we do not expect the quantitative values to match. (1) The criteria used to assess critical sample spacing and grating acuity differ. (2) The nonlinear regression model makes a cautious, conservative estimate of sample spacing. (3) Critical sample spacing is presumably a manifestation of filtering by the optics and photoreceptors alone while grating acuity manifests the properties of the visual system as a whole.

and 5 minarc correspond with spatial frequencies of 30 and 12 c/deg, respectively. Thus, we observed responses to spatial frequencies, resulting from the spatial sampling in the stimulus, that are significantly higher than the grating acuities measured in the same infants. This disparity between the spatial frequencies that can cause threshold elevation and those that can drive an evoked response directly suggests strongly that the optics and photoreceptors of the young eye transmit spatial detail that is subsequently lost in the retina and central visual pathways. This observation is reminiscent of some observations of peripheral vision in human adults, where optical quality is also better than neural resolving power (Thibos, Walsh & Cheney, 1987; Anderson & Hess, 1990). Now that it has been shown that the primary loss in human infants is not at the optics or the collecting aperture of the receptors, an important topic for future research is to determine where in the visual pathway the loss of high spatial frequency information occurs.

There is a remarkable aspect of our infant data that warrants comment. With the adult observers, we paralyzed accommodation via cycloplegia and then corrected any residual refractive error optically. The optical correction was important for obtaining a precise measure of critical sample spacing as evidenced by the fact that introducing two diopters of defocus increased critical spacing from 2 to 6 minarc, a three-fold increase (Fig. 7). In contrast, the infants were not cyclopleged or corrected optically so they freely accommodated during the course of the experiments. Nonetheless, we observed threshold elevations with sample spacing as small as 2–3 minarc. Accommodative defocus would have the effect of increasing the estimated critical sample spacing relative to the best possible critical spacing. Thus, with precise optical correction, we might have observed even smaller critical sample spacings in infants[7].

7.2. Comparison of our findings with previous work

Infants' visual acuity and contrast sensitivity are distinctly lower than adults', but those measures of visual sensitivity improve rapidly during the first year of life. Consistent with this general statement, we observed grating acuities of 2–10 c/deg in infants from 2 to 7 months of age. An important question is, What part or parts of the visual process are primarily responsible for this poor sensitivity early in life?

Numerous modeling efforts have addressed this question. It is well known that foveal cones and the arrangement of those cones are quite immature during the first months of life (Yuodelis & Hendrickson, 1986). Therefore, the modeling efforts have focused on the question of how front-end factors (optics, photoreceptor properties, and receptor lattice properties) limit visual sensitivity in the young visual system. Nearly all have concluded that these factors are a significant limit to sensitivity, but most have concluded that they are not the only mechanism responsible for low visual sensitivity early in life (Banks & Bennett, 1988; Brown et al., 1987; Banks & Crowell, 1993; Brown, 1993; but see Wilson, 1988, 1993).

The data reported here seem to suggest that very little of the deficit in visual resolution is attributable to the first linear filter which assuredly incorporates both the optics and photoreceptors (at least up to the point of isomerization). Consequently, our data might seem to conflict with the modelers' conclusion that immaturities among the optics, photoreceptors, and receptor lattice significantly limit performance in the young visual system. Fortunately, this is not the case, for the following reasons. The models assume (e.g. Banks & Bennett, 1988) that the infant's optics are nearly adult-like, so the primary consequence of the front-end immaturities is a reduction in the number of photons effectively absorbed in the photoreceptor array. This reduced photon catch causes the models to predict lower contrast sensitivity. A byproduct of lower contrast sensitivity is a reduction in visual acuity. Our infant threshold data were collected at fixed spatial frequencies. Comparison of the unnormalised data in Figs. 8 and 9 shows that the infant thresholds were at least 0.5 log unit higher than the adult thresholds; this observation is consistent with the conclusions of the earlier models. Our key measurement in the present work, however, was the change in threshold due to changes in sample spacing. As we argued earlier, the spacing at which threshold elevation occurs is a measure of the span of the first linear filter, but not of the sensitivity of that filter (in the signal-to-noise sense) nor of the sensitivity of the rest of the visual system. Thus, the finding that the span of the first linear filter is similar in adults and infants is not inconsistent with the earlier conclusion that photoreceptor immaturities affect visual sensitivity.

7.3. Aliasing and interpretation of the data

When an image contains information finer than the element spacing in a sampling array, spatial distortions or aliases are created. The spatial frequencies of the aliases can be much lower than the image frequencies themselves. Specifically, the arrangement of the sampling array defines the highest spatial frequency that can be represented without aliasing intruding within the range of frequencies nominally contained in the image; this highest frequency is the Nyquist frequency. The problem of aliasing is avoided in the adult fovea be-

[7] Infants accommodate accurately at our viewing distance of 1 m (Aslin, 1993).

cause the optics do not pass spatial frequencies higher than the Nyquist frequency; one needs to bypass optical degradation in order to see aliasing due to photoreceptor sampling (Williams, 1985). In human neonates, it is possible that the spatial frequencies in the retinal image can exceed the Nyquist frequency of the photoreceptor lattice. In particular, the optics seem to be nearly adult-like (e.g. Cook & Glasscock, 1951) while the spacing among foveal cones is much coarser than in adults (Yuodelis & Hendrickson, 1986). According to the best current estimate of receptor spacing (Candy, Crowell & Banks, 1998), the sampling frequency of the infant foveal receptor lattice is 27 c/deg, so the Nyquist frequency is 13.5 c/deg. Here we have found visual responses generated by spatial frequencies higher than that. Could the production of spatial aliases due to undersampling of the retinal image have affected our data?

Our stimuli consisted of sampling components (triplets at each multiple of the sampling frequency), the fundamental (the signal in the experiment), and a DC component. One can calculate the spatial frequencies of potential aliases from the stimulus component frequencies and the receptor sampling frequency. Many of the hypothetical aliases would be too high in spatial frequency to have influenced the VEP signal, but some could have low spatial frequency. Some of the potentially low-frequency aliases (the ones arising from receptor sampling of the unmodulated sampling components) would not be modulated at the temporal frequency of our stimulus and, therefore, would not be modulated at the temporal frequency analysed in the VEP. Others (arising from receptor sampling of the sidebands of the sampling components) would be modulated at the temporal frequency of the stimulus. Could those hypothetical aliases affect our data by masking the response to the modulation of the sinewave? We think not for two reasons. First, the amplitude of any aliases created by the receptor lattice sampling ought to be very low in infants because they were free to move their eyes and eye movements cause spatial aliases to appear at very high temporal frequencies. Second, the infant receptor lattice is probably at least as irregular as the adult lattice (and lattice irregularity attenuates the amplitude of spatial aliases; Yellott, 1983). We conclude, therefore, that spatial aliases created by undersampling by the photoreceptor lattice would almost certainly not have affected our threshold data.

Although aliasing effects on our data seem very unlikely, corruption by aliasing would not invalidate our conclusion concerning the optics of the infant eye. Aliasing is a consequence of discrete sampling by the receptors or higher-order neurons, so high-frequency information must reach the receptors in order to produce an alias. In other words, the optics must pass the sampling frequency for the threshold elevation to occur so the relationship between the optics and critical sample spacing would not be affected by aliasing anyway.

7.4. Concluding remarks

Using a stimulus developed by Burr et al. (1985), we examined the resolution of visual processes anterior to the first nonlinearity. Ancillary experiments in adults confirmed that the sample spacing at which threshold elevation occurs is a manifestation of the resolution of pre-nonlinearity processes which are presumably the optics and photoreceptors. In our infant experiment, we observed threshold elevations at sample spacings whose equivalant spatial frequencies were significantly higher than the frequencies that can themselves drive a VEP. The disparity between the spatial frequencies that can cause threshold elevation and those that can drive an evoked response suggests strongly that the optics and photoreceptors of the young eye transmit spatial information that is subsequently lost in the retina and central visual pathways. An important topic for future research is to determine where in the visual pathway the loss of high spatial frequency information occurs.

Acknowledgements

This work was supported by a William C. Ezell Fellowship from the American Optometric Foundation and the UC Berkeley Elizabeth Roboz Einstein Fellowship in developmental neuroscience awarded to TRC, by research grants from NIH (HD-19927 awarded to MSB, and EY-06579 awarded to A.M. Norcia) and by the Max-Planck Institute for Biological Cybernetics, Tübingen, Germany. We thank Anthony Norcia and Kirk Swenson for assistance in creating the experimental displays and Sarah Freeman, Sharyn Gillett, and Jeong-Ah Kim for assistance with testing infants.

References

Aslin, R. N. (1993). Infant accommodation and convergence. In K. Simons, *Early visual development: normal and abnormal*. New York: Oxford University Press.

Anderson, S. J., & Hess, R. F. (1990). Post-receptoral undersampling in normal human peripheral vision. *Vision Research*, *30*, 1507–1515.

Banks, M. S., & Bennett, P. J. (1988). Optical and photoreceptor immaturities limit the spatial and chromatic vision of human neonates. *Journal of the Optical Society of America*, *5*, 2059–2079.

Banks, M. S., & Crowell, J. A. (1993). A re-examination of two analyses of front-end limitations to infant vision. In K. Simons, *Early visual development: normal and abnormal*. New York: Oxford University Press.

Banks, M. S., Sekuler, A. B., & Anderson, S. J. (1991). Peripheral spatial vision: limits imposed by optics, photoreceptors, and receptor pooling. *Journal of the Optical Society of America A*, *8*, 1775–1787.

Brown, A. M., Dobson, V., & Maier, J. (1987). Visual acuity of human infants at scotopic, mesopic and photopic luminances. *Vision Research*, *27*, 1845–1858.

Brown, A. M. (1993). Intrinsic noise and infant visual performance. In K. Simons, *Early visual development: normal and abnormal*. New York: Oxford University Press.

Burr, D. C., Ross, J., & Morrone, M. C. (1985). Local regulation of luminance gain. *Vision Research*, *25*, 717–727.

Burton, G. J. (1973). Evidence for nonlinear response processes in the human visual system from measurement on the thresholds of spatial beat frequencies. *Vision Research*, *13*, 1211–1225.

Campbell, F. W., & Gubisch, R. W. (1966). Optical quality of the human eye. *Journal of Physiology*, *186*, 558–578.

Candy, T. R., Banks, M. S., Hendrickson, A. E., & Crowell, J. A. (1993). Neonatal vision and cone properties in fovea and periphery. *Investigative Ophthalmology and Visual Science* (*Supplement*), *34*, 1356.

Candy, T. R., Crowell, J. A., & Banks, M. S. (1998). Optical, receptoral, and retinal constraints on foveal and peripheral vision in the human neonate. *Vision Research*, *38*, 3857–3870.

Chen, B., Makous, W., & Williams, D. R. (1993). Serial spatial filters in vision. *Vision Research*, *33*, 413–427.

Cook, R. C., & Glasscock, R. E. (1951). Refractive and ocular findings in the newborn. *American Journal of Ophthalmology*, *34*, 1407–1413.

Curcio, C. A. (1987). Diameters of presumed cone apertures in human retina. In *Annual Meeting of the Optical Society of America* (pp. 1–11).

Green, D. M. (1976). *An introduction to hearing*. New Jersey: Lawrence Erlbaum.

Jasper, H. H. (1958). The ten-twenty electrode system of the international federation. *Electroencephalography and Clinical Neurophysiology*, *10*, 371–375.

Klein, S. A., Hu, Q. J., & Carney, T. (1996). The adjacent pixel nonlinearity: problems and solutions. *Vision Research*, *36*, 3167–3181.

Lam, D. M.-K., & Shatz, C. J. (1991). *Development of the visual system*. Cambridge: MIT.

Levi, D. M., & Klein, S. A. (1990). Equivalent intrinsic blur in spatial vision. *Vision Research*, *30*, 1971–1993.

MacLeod, D. I. A., Williams, D. R., & Makous, W. (1992). A visual nonlinearity fed by single cones. *Vision Research*, *32*, 347–363.

MacLeod, D. I., & He, S. (1993). Visible flicker from invisible patterns. *Nature*, *361*, 256–258.

Navarro, R., Artal, P., & Williams, D. R. (1993). Modulation transfer of the human eye as a function of retinal eccentricity. *Journal of the Optical Society of America A*, *10*, 201–212.

Norcia, A. M., Clarke, M., & Tyler, C. W. (1985). Digital filtering and robust regression techniques for estimating sensory thresholds from the evoked potential. *IEEE Engineering in Medicine and Biology Magazine*, *4*, 26–32.

Norcia, A. M., & Tyler, C. W. (1985). Spatial frequency sweep VEP: visual acuity during the first year of life. *Vision Research*, *25*, 1399–1408.

Norcia, A. M., Tyker, C. W., & Hamer, R. D. (1990). Development of contrast sensitivity in the human infant. *Vision Research*, *30*, 1475–1486.

Norcia, A. M., Tyler, C. W., Hamer, R. D., & Wesemann, W. (1989). Measurement of spatial contrast sensitivity with the swept contrast VEP. *Vision Research*, *29*, 627–637.

Pelli, D. G., & Zhang, L. (1991). Accurate control of contrast on microcomputer displays. *Vision Research*, *31*, 1337–1350.

Sokol, S., Moskowitz, A., McCormack, G., & Augliere, R. (1988). Infant grating acuity is temporally tuned. *Vision Research*, *28*, 1357–1366.

Stromeyer, C. F., & Julesz, B. (1972). Spatial-frequency masking in vision: critical bands and spread of masking. *Journal of the Optical Society of America*, *62*, 1221–1232.

Teller, D. Y. (1979). The forced-choice preferential looking procedure: a psychophysical technique for use with human infants. *Infant Behavior and Development*, *2*, 135–153.

Thibos, L. N., Walsh, D. J., & Cheney, F. E. (1987). Vision beyond the resolution limit: aliasing in the periphery. *Vision Research*, *27*, 2193–2197.

Wässle, H., Grünert, U., Röhrenbeck, J., & Boycott, B. B. (1990). Retinal ganglion cell density and cortical magnification factor in the primate. *Vision Research*, *30*, 1897–1911.

Williams, D. R. (1985). Visibility of interference fringes near the resolution limit. *Journal of the Optical Society of America A*, *2*, 1087–1093.

Wilson, H. R. (1988). Development of spatiotemporal mechanisms in infant vision. *Vision Research*, *28*, 611–628.

Wilson, H. R. (1993). Theories of infant visual development. In K. Simons, *Early visual development: normal and abnormal*. New York: Oxford University Press.

Yellott, J. I. Jr. (1983). Spectral consequences of photoreceptor sampling in the rhesus retina. *Science*, *221*, 382–385.

Yuodelis, C., & Hendrickson, A. E. (1986). A qualitative and quantitative analysis of the human fovea during development. *Vision Research*, *26*, 847–855.